Localization by bichromatic potentials versus Anderson localization

Mathias Albert and Patricio Leboeuf
Laboratoire de Physique Théorique et Modèles Statistiques, CNRS, Université Paris Sud, UMR8626, F-91405 Orsay Cedex, France
(Received 14 May 2009; published 19 January 2010)

The one-dimensional propagation of waves in a bichromatic potential may be modeled by the Aubry-André Hamiltonian. This, in turn, presents a localization transition that has been observed in recent experiments using ultracold atoms or light. It is shown here that, in contrast to the Anderson model, the localization mechanism has a classical origin, namely it is not due to a quantum suppression of a classically allowed transport process, but rather is produced by a trapping by the potential. Explicit comparisons with the Anderson model as well as with experiments are presented.

DOI: 10.1103/PhysRevA.81.013614 PACS number(s): 67.85.−d, 72.15.Rn, 03.65.Sq

I. INTRODUCTION

It is by now well established that disorder may lead to the absence of diffusion in the propagation of linear waves (Anderson localization). The phenomenology of Anderson localization strongly depends on dimensionality. In one-dimensional (1D) and uncorrelated disorders it has been shown that all wave functions are exponentially localized. This implies that the transmission of a wave packet incident on a disordered region of length L decreases as $\exp(-L/L_{\mathrm{loc}})$, where $L_{\mathrm{loc}} \ll L$ is the localization length. This phenomenon is valid for arbitrary energies, even when the energy E of the incident wave packet is much higher than the highest barrier of the disordered potential. In this respect, Anderson localization is a strongly nonclassical phenomenon.

Another class of interesting potentials are quasiperiodic potentials. They arise, typically, from the superposition of two periodic lattices with incommensurate periods. Part of their interest is that they provide an example of intermediate potentials between ordered (e.g., periodic) and disordered potentials: The system has neither translational symmetry nor true disorder. In particular, the model we consider here (the Aubry-André Hamiltonian) is known to present a localization transition as a parameter varies; thus wave functions change from extended to exponentially localized [1].

In recent experiments both random [2] and quasiperiodic potentials [3] were used to directly observe the localization of matter waves. The expansion of noninteracting Bose-Einstein condensates through one-dimensional quasiperiodic potentials was shown to clearly display a delocalized-localized crossover (with a shift, however, with respect to the predicted critical value of the parameter) [3]. A similar transition was recently observed with light propagating in quasiperiodic photonic lattices [4]. Our purpose here is to provide a semiclassical analysis of the experiments and, more generally, of the Aubry-André Hamiltonian, which allows for a simple and lucid picture of the underlying physical phenomena (for related semiclassical analysis see, e.g., Refs. [5–10]). In particular, and in contrast to what is quite often claimed, the analysis shows that there are deep fundamental differences between the Anderson localization and the localization in quasiperiodic potentials, although both present exponential localization of the wave functions.

As already pointed out, Anderson localization is a strongly nonclassical phenomenon where a quantum particle of energy E incident on a 1D disordered region of length $L \to \infty$ is reflected with probability one even though its incident energy is much higher than the maximum height of the disordered potential. Thus, in Anderson localization a quantum particle is perfectly reflected, whereas its classical counterpart is perfectly transmitted. In this sense, Anderson localization is a purely wave-mechanical effect. In contrast, as shown in the following, localization in quasiperiodic potentials is different. It is a purely classical effect due to the trapping of the particle by the potential barriers. It is not due to a destructive interference process. Quantum mechanically, there is thus no suppression of a classical diffusive process. Moreover, the delocalized phase of the model corresponds to classical trajectories with a kinetic energy higher than the potential. Thus, in this integrable model the wave functions, quantized through a Wentzel-Kramers-Brillouin (WKB) semiclassical approximation, simply follow the classical behavior. It is our purpose to stress these aspects of the model and to clarify the connections with recent experiments.

II. THE MODEL

The Hamiltonian we are interested in is of the tight-binding form with nearest-neighbor hopping between discrete position sites q_n and a superimposed quasiperiodic potential

$$\hat{H} = J \sum_n (|q_{n+1}\rangle\langle q_n| + |q_n\rangle\langle q_{n+1}|) + W \sum_n \cos(2\pi\beta n)|q_n\rangle\langle q_n|, \quad (1)$$

where β is the commensurability parameter, $|q_n\rangle$ is a localized Wannier state on site n of the lattice, and J and W are parameters that control the amplitude of the hopping transitions and of the quasiperiodic potential, respectively. Since the Hamiltonian is invariant under the increase of β by an arbitrary integer, we can restrict it to $0 < \beta \leqslant 1$. This Hamiltonian is known as the Aubry-André or Harper Hamiltonian in the literature [1,11]. There are two well-known physical problems effectively described by Eq. (1). The first is the motion of electrons in two dimensions for a periodic potential in the presence of a magnetic field applied perpendicular to the plane when interband transitions are neglected [12]. In this case, β is related to the ratio of the area of the magnetic flux quantum to the unit cell in coordinate space. The second, directly related to the experiments described here, is the 1D motion of particles in

 ©2010 The American Physical Society

the presence of two superimposed periodic potentials, the main one of period λ_1 that determines the position of the discrete lattice points q_n and the perturbing one of period λ_2; in this case $\beta = \lambda_1/\lambda_2$. The connection between the latter problem and Eq. (1) is explicitly described in the next section and in Appendix A.

Expressing the hopping between nearest-neighbor sites of the main lattice in terms of the translation operator $\exp(-i\lambda_1\hat{p}/\hbar)$ ($\hat{q}$ and $\hat{p}$ are the usual position and momentum operators, respectively), one can transform Eq. (1) into the more symmetric form

$$\hat{H} = 2J\cos(2\pi\hat{p}/P) + W\cos(2\pi\hat{q}/Q), \tag{2}$$

where $P = 2\pi\hbar/\lambda_1$ and $Q = \lambda_2$. The classical analog of this Hamiltonian is obtained by replacing the operators by c numbers

$$\mathcal{H}(q, p) = 2J\cos(2\pi p/P) + W\cos(2\pi q/Q). \tag{3}$$

This classical Hamiltonian is periodic in both position and momentum. Therefore, its study can be restricted to a single cell of size (Q, P). Note that $\mathcal{H}(q, p)$ contains, through the momentum scale factor $P = h/\lambda_1$, quantum Planck's constant. Its validity and applicability as well as the apparent paradox that it contains a quantum scale will be discussed.

$\mathcal{H}(q, p)$ defines a time-independent 1D problem that conserves the energy. It is thus an integrable system with Eq. (3) defining, for different values of the energy $E = \mathcal{H}(q, p)$, 1D curves in the phase-space plane (q, p). The classical phase-space dynamics is sketched in Fig. 1 for different values of $\alpha = W/J$. For $\alpha = 0$ there is no potential and all trajectories are extended in space, a simple ballistic motion (e.g., the projection of the classical curves onto the q axis covers the entire interval $[0, Q]$, in contrast to localized orbits that cover only a fraction of it) and have constant momentum. For $\alpha \gg 1$

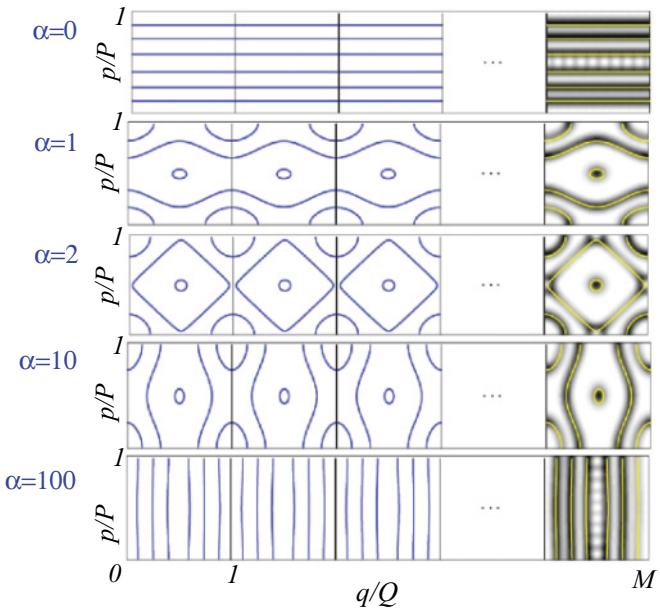

FIG. 1. (Color online) Phase-space trajectories of Hamiltonian (3) for different values of the parameter $\alpha = W/J$ solid lines. In the right-hand column, the Husimi representation of several eigenstates for $\beta = 1/51$ is superimposed on the classical trajectories (see text).

exactly the opposite happens; the potential part dominates, the kinetic energy becomes negligible, and trajectories are trapped or localized in space by the potential and delocalized in momentum. This latter behavior is a consequence of the boundedness of the kinetic term. In between, a crossover is observed with the presence of two separatrices that delimit three different types of trajectories. The first type are closed localized orbits that oscillate around $(q, p) = (Q/2, P/2)$. This is a standard clockwise oscillation around the minimum of $\cos(2\pi q/Q)$. The second type is also a closed localized oscillation, now around $(q, p) = (0, 0), \mathrm{mod}(Q, P)$, which is a less standard counterclockwise oscillation around the maximum of $\cos(2\pi q/Q)$ due to a local negative mass. Finally, the third type, in between the separatrices, is an extended orbit in q for $\alpha < 2$ and p for $\alpha > 2$. At $\alpha = 2$ the two separatrices merge together. This is the critical value of the parameter α above which the potential part dominates over the kinetic one and all classical trajectories are localized in space by the potential barriers.

The quantum-mechanical motion is richer than the classical one as a result of the additional parameter $\beta = \lambda_1/\lambda_2 = 2\pi\hbar/QP$. Its presence in the quantum Hamiltonian is a consequence of the discrete nature of the motion in the q direction, defined by the position of the main lattice sites and the commensurability effects with respect to the secondary lattice. The quantum operator Eq. (2) commutes with the translation operators $\hat{T}_Q = \exp(-iQ\hat{p}/\hbar)$ and $\hat{T}_P = \exp(iP\hat{q}/\hbar)$, which translate by one unit cell in each phase-space direction. However, quantum dynamics simultaneously periodic in both directions, as in the classical one, are possible if and only if the translation operators also commute with each other. The most general condition enforces commutation by translations over a phase-space domain of dimensions (MQ, P), where M is an arbitrary positive integer. It is easy to show [9] that the operators T_{MQ} and T_P commute if and only if β is a rational number

$$\frac{1}{\beta} = \frac{QP}{2\pi\hbar} = \frac{N}{M}, \tag{4}$$

where N is an arbitrary positive integer. Keeping in mind the old Weyl rule "one quantum state per phase-space volume h," the physical interpretation of this condition is clear: To be periodic in both directions, the extended phase-space cell (MQ, P) made of M units in the q direction should contain an integer number N of quantum states. This defines the torus (MQ, P) as the quantum phase space. An arbitrary quantum state now satisfies the generalized boundary conditions

$$\begin{aligned} T_{MQ}|\psi\rangle &= e^{i\theta_1}|\psi\rangle, \\ T_P|\psi\rangle &= e^{i\theta_2}|\psi\rangle, \end{aligned} \tag{5}$$

where $\vec{\theta} = (\theta_1, \theta_2)$ are good quantum numbers preserved by the dynamics (the Bloch phases). Hence the Hilbert space breaks down into N-dimensional subspaces parametrized by $\vec{\theta}$. $\hat{H}$ is therefore a finite-dimensional periodic operator where the spectrum is absolutely continuous. The latter term consists of N Bloch bands $E_i(\vec{\theta})$, defined by

$$\hat{H}|\psi_i(\vec{\theta})\rangle = E_i(\vec{\theta})|\psi_i(\vec{\theta})\rangle \quad i = 0, \ldots, N-1, \tag{6}$$

where $|\psi_i(\vec{\theta})\rangle$ are the eigenvectors that satisfy Eq. (5). Strictly speaking, due to the periodicity all eigenstates are thus delocalized for any value of the parameter α.

Note that the semiclassical limit is obtained when $N \to \infty$, that is, when the number of quantum states is large (possibly with $M \to \infty$ but $M/N \to 0$). In this case the fraction of phase space occupied by one quantum state tends to zero and the quantum dynamics is described with increasing precision by the classical Hamiltonian, Eq. (3). The semiclassical limit is thus equivalent to the limit $\beta \to 0$ (or, more generally, due to the periodicity, to the limit β tending to an arbitrary integer from above). In practice, β plays the role of an effective Planck's constant. Since $\beta = \lambda_1/\lambda_2$, an appropriate choice for the period of the two superimposed periodic potentials allows to tune β and control whether the system is quantum or classical. This limit is thus different from the usual semiclassical limit, where one formally takes $\hbar \to 0$ or considers a high-energy regime. From this point of view, there is no contradiction in the fact that the classical Hamiltonian $\mathcal{H}(q, p)$ contains h since the path toward the classical behavior described by that Hamiltonian is controlled by the two frequencies λ_1 and λ_2. This emphasizes that the classical limit $\beta \to 0$ that we are considering has a more general character. It is one example among a wider class of semiclassical limits, sometimes generically called large-N limits, that are often encountered in physics (see, for instance, Ref. [13] and references therein). In our case, the classical limit does not correspond to the standard limit of a classical particle of kinetic energy $p^2/2m$ moving in the presence of two superimposed periodic potentials [cf. Eq. (10)]. Although purely classical, the structure of $\mathcal{H}(q, p)$ keeps information about some of the quantum mechanical processes associated to the original model, Eq. (1). The periodicity in the p direction arises from the discreteness of the lattice sites distant by λ_1 imposed by the tight-binding form of the dynamics related to a tunneling process. As mentioned earlier, the boundedness of the kinetic energy term has important consequences, in particular in the appearance of the unusual localized-in-space delocalized-in-momentum classical trajectories observed in the limit of a large α.

Now we turn to the case of irrational β, the quantum-mechanical behavior of which deserves special attention. Contrary to our previous discussion, in this case the phase space is not compact, the Bloch angles are not good quantum numbers, and the matrix $\hat{H}$ is of infinite dimension. For any irrational value of β it can be shown [14] that the spectrum is a Cantor set (among which is the famous Hofstadter butterfly for $\alpha = 2$). In addition, the model displays a localization transition [1,15]. For $\alpha < 2$, the spectrum is absolutely continuous and all states are extended. For $\alpha > 2$, the spectrum is pure point and all states are localized. Finally, at $\alpha = 2$ the spectrum is singular continuous with multifractal eigenstates [1].

The ideal situation concerning any physical experiment, the aim of which is to display the localization transition, is to implement an irrational β, typically the golden mean $(\sqrt{5} - 1)/2$. In practice, one can only approach an irrational as some rational approximation. It is thus of interest to analyze an irrational β as the limit of a sequence of rational numbers. The most efficient sequence (in terms of convergence) is known to be the continuous fraction expansion

$$\beta = \cfrac{1}{m_1 + \cfrac{1}{m_2 + \cfrac{1}{m_3 + \cdots}}}. \tag{7}$$

This sequence of rational approximations $\beta_1 = 1/m_1$, $\beta_2 = m_2/(m_1 m_2 + 1)$, and so on generates a sequence of periodic systems that approximate the quasiperiodic one with increasing accuracy. In the lowest-order approximation $\beta_1 = 1/m_1$, only one unit cell is quantized ($M = 1$), with $N = m_1$ quantum states supported by this cell. For such a situation, the WKB method semiclassically allows us, in 1D, to construct the eigenstates $\psi_i(\vec{\theta})$ and eigenvalues $E_i(\vec{\theta})$ from the quantization of some specific classical trajectories in a one-to-one correspondence. The m_1 states are selected by the Bohr-Sommerfeld quantization rule [16]

$$S = \int_t p dq = \beta Q P \left[i + \left(\frac{1}{2} \right) + w_1 \frac{\theta_1}{2\pi} + w_2 \frac{\theta_2}{2\pi} \right], \tag{8}$$

where $i = 0, \ldots, m_1$, (w_1, w_2) are the winding numbers of the quantized classical trajectory t in the (q, p) directions, respectively, and $S = S(E)$ is the action of t. The Maslov index half applies only to trajectories with $(w_1, w_2) = (0, 0)$ (closed trajectories). The eigenvalues of states associated to $(0, 0)$ trajectories are thus, at this semiclassical level of approximation, independent of $\vec{\theta}$.

Equation (8) associates one quantum state to one classical trajectory of the elementary phase-space cell and defines the spectrum of energies $E_i(\vec{\theta})$. In this description, the associated quantum state $\psi_i(\vec{\theta})$ can be shown to strongly concentrate or localize around the corresponding quantized classical trajectory. To illustrate this point it is useful to display the eigenstates in the phase-space Husimi representation [9], defined in Appendix B. In this representation, each eigenstate $\psi_i(\vec{\theta})$ of energy $E_i(\vec{\theta})$ corresponds to a positive-definite phase-space function $W_i(q, p; \vec{\theta})$, which, in the semiclassical limit $1/\beta_1 = m_1 \to \infty$, behaves as [10]

$$W_i(q, p; \vec{\theta}) \propto \frac{1}{v(q, p)} \exp \left[-\frac{2}{m_1} \left(\frac{\mathcal{H}(q, p) - E_i(\vec{\theta})}{v(q, p)} \right)^2 \right], \tag{9}$$

where $v(q, p) = \sqrt{\dot{q}^2 + \dot{p}^2}$ is the phase-space velocity of the classical trajectory of energy E_i. The right-hand column of Fig. 1 superimposes on the classical trajectories the corresponding quantized eigenstates for $N = m_1 = 51$, $M = 1$, $\vec{\theta} = (0, 0)$, and different values of α. One can clearly see that, for a given α, the concentration over the corresponding classical trajectory as well as, for varying α, the transition from extended to localized states, which simply follow the classical crossover (e.g., localization by the potential barriers). For open trajectories (either in the q direction for $\alpha < 2$ or in p for $\alpha > 2$) the quantum state is supported by two symmetric and isoenergetic classical curves coupled by tunneling. This effect is observed at $\vec{\theta} = (0, 0)$ where the eigenstates are real. The quantum state combines both classical trajectories, each of which has a current but whose overall superimposed net current vanishes. As $\vec{\theta}$ is varied, the eigenstate becomes complex and can concentrate on one or the other of the classical trajectories.

At the second step of the rational approximation to an irrational β, $\beta \approx \beta_2 = m_2/(m_1 m_2 + 1)$, the quantum phase space is an extended torus of dimensions $(m_2 Q, P)$. This space now supports $N = m_1 m_2 + 1$ quantum states. With respect to the previous approximation $\beta \approx \beta_1 = 1/m_1$, the

size of the quantum cell and the number of states $N \approx m_1 m_2$ increases by a factor m_2; in contrast, the number of quantum states per unit of phase-space cell remains almost constant. The scheme repeats as one further increases the order of the continuous-fraction approximation. Along this process, the size of the extended phase-space cell increases in the q direction (thus tending toward a cylindrical geometry); the dimension of the corresponding Hilbert space also increases, while the effective Planck constant β, which measures the fraction of the elementary phase-space cell occupied by one quantum state remains approximately constant. At a given step of the approximation and a given $\vec{\theta}$, it can be shown from Eq. (8) that two types of quantum states exist classified according to the structure of the wave function in the extended phase space (MQ, P). First, the delocalized ones, which are associated to classical orbits open in the q direction of the $(\pm 1, 0)$ type with a kinetic energy higher than the potential barriers (that exist only for $\alpha < 2$). Second, localized states associated to either closed orbits [of the $(0, 0)$ type] or to open orbits in the p direction [of the $(0, \pm 1)$ type], in other words, orbits that are trapped by the potential barriers. These states are typically localized over one (or several, when resonances occur) isoenergetic classical orbits of the extended phase space. Their width, controlled by β, remains almost constant along the continuous-fraction approximation. Thus, as the size of the extended torus increases in the q direction, the relative width of the localized states compared to MQ diminishes. Husimi plots of wave functions that confirm our general picture can be found in Ref. [17] for sequences of rational approximations of the golden mean.

III. RELATION TO EXPERIMENTS

In recent experiments [3], a cloud of noninteracting ultracold ^{39}K atoms created from a Bose-Einstein condensate is released in a bichromatic potential produced by superimposing two lasers of wavelengths λ_1 and λ_2 (and of corresponding wave numbers k_1 and k_2) in a standing-wave configuration. The dynamics is described by the following Hamiltonian

$$\hat{H}_B = -\frac{\hbar^2}{2m}\frac{\partial^2}{\partial x^2} + V_1 \cos^2(k_1 x) + V_2 \cos^2(k_2 x), \quad (10)$$

where V_1 and V_2 denote the amplitude of each of the two laser beams and m is the mass of the atom. If the primary lattice (say, V_1) is deep enough, that is if the recoil energy $E_R = \hbar^2 k_1^2/2m$ is much lower than V_1, one can approximate the motion in the primary lattice using a tunneling process between localized states of neighboring sites, each of which feels the presence of the superimposed additional periodic potential V_2. The Hamiltonian can thus be reduced to the tight-binding form of Eq. (1) where $\beta = \lambda_1/\lambda_2$. The effective parameters J and W in Eq. (1) are directly related to V_1, V_2, and E_R (see Appendix A).

Several different laser frequencies were used in the experiments. In Ref. [3] they realized the system described by the Hamiltonian (10) with $\lambda_1 = 1032$ nm and $\lambda_2 = 862$ nm, which yields $\lambda_1/\lambda_2 = 516/431$ (431 is a prime number). By restricting to $0 < \beta \leqslant 1$, we have $\beta = 85/431 \simeq 0.1972$. Moreover, the typical amplitude of the primary lattice is ten times larger than the corresponding recoil energy, which makes Eq. (1) a good approximation to the experiment. With the above values of λ_1, λ_2, and β the quantum system under study is therefore periodic in both q and p directions (because β is rational), with $N = 431$ states accommodated in $M = 85$ elementary cells. This means that every 431 wells of the primary lattice the system repeats. The Hamiltonian (1) is thus a finite matrix of dimension $N = 431$ and the eigenvalues and eigenstates depend parametrically on the two phases $\vec{\theta} = (\theta_1, \theta_2)$. It can be shown (see Ref. [9] and Appendix B) that the two phases are determined by the relative position of the two lattice sites. Though not directly measured in the previous experiments, the Bloch phases are fixed by the experimental conditions. To be specific, we fix them here to $\vec{\theta} = (0, 0)$. Coming back to β, its continuous-fraction decomposition gives two lower-order approximants, $\beta_1 = 1/5$ and $\beta_2 = 14/71$. The system is thus nearly periodic after five wells of the primary lattice. The approximation $\beta \sim \beta_1$ also means that approximately five quantum states are accommodated in one elementary phase-space cell (Q, P). Moreover, the relatively low value of $\beta \approx 0.2$ indicates that the classical approximation of the dynamics given by Eq. (3) as well as the the semiclassical picture developed in the previous section is a meaningful framework, as discussed in the following.

Figure 2 shows the Husimi function of several eigenstates of Eq. (1) represented in the quantum phase space (MQ, P) for the experimental conditions, namely $\beta = 85/431$, and different values of α, assuming $\vec{\theta} = (0, 0)$. One verifies

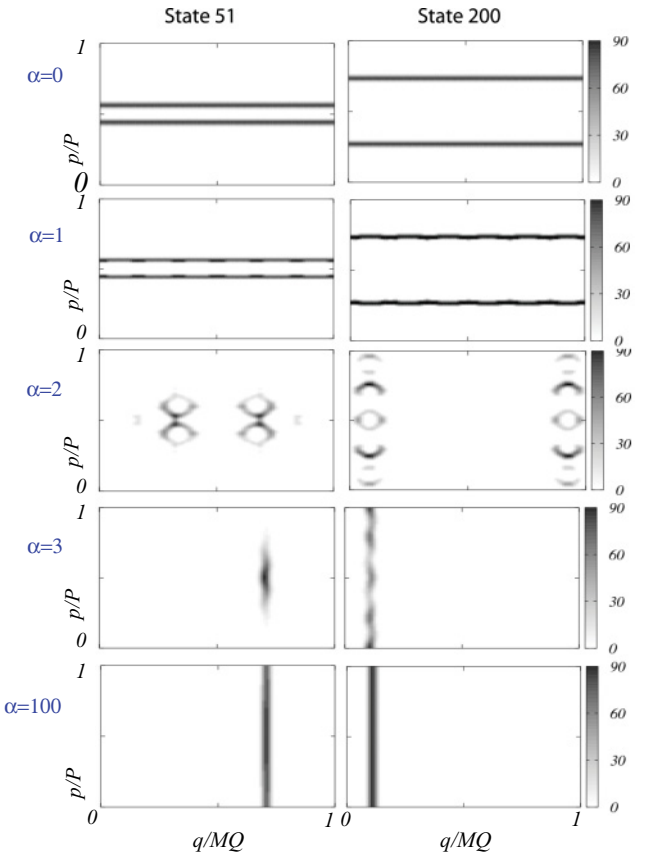

FIG. 2. (Color online) Husimi functions for $N = 431$ and $M = 516$ for two arbitrary quantum states as a function of α. Their evolution clearly illustrates the delocalized-localized crossover.

that the eigenstates follow, for different α's, the general description given at the end of the last section. For $\alpha \ll 2$ the eigenstates are concentrated along the delocalized classical trajectories [mixing right and left-propagating orbits because $\vec{\theta} = (0, 0)$] while for $\alpha \gg 2$ the eigenstates are concentrated on localized trajectories that wind around in the p direction. In between, a crossover among these two limits is observed. This figure illustrates, under the experimental conditions, that the transition from delocalized to localized states as α increases may be interpreted in terms of classical dynamics and is therefore different in nature from the Anderson localization. Moreover, as already pointed out in the introduction, this behavior is generic and not restricted to the special set of parameters used in the experiment.

Experimentally, the transition was probed through the evolution of different values of α of an initial cloud of atoms released from the ground state of a confining magnetic trap. The initial state is thus a Gaussian wave packet centered around some initial point q_0 and contains zero average initial momentum with an extension of about ten main lattice sites. After letting the cloud expand for some time (750 ms), the final root-mean-square (RMS) width of the wave packet is measured. These results are reported in Fig. 3. To test our setting, we computed, using the eigenstates discussed earlier, the time evolution $|\phi(t)\rangle$ of such an initial state, given by

$$|\phi(t)\rangle = \sum_{i=0}^{N-1} \exp[-iE_i(\vec{\theta})t/\hbar]\overline{\psi}_i(z_0)|\psi_i(\vec{\theta})\rangle, \qquad (11)$$

where, for the actual experiment, $N = 431$, $\overline{\psi}_i(z_0)$ is the coherent-state representation of the eigenstate i, where $z_0 = q_0/\sqrt{2}$ (cf. Appendix B), and the Bloch angles $\vec{\theta}$ are set to zero. In Fig. 3 the width averaged over the initial position computed from Eq. (11) (dashed-dot line) is compared to the experimental data. The agreement is quite good. Note that the transition takes place here for $\alpha \approx 2$, as predicted by theory, and not around $\alpha \approx 7$, as obtained in Ref. [3]. The difference is due to an improved estimate of the dependence of the effective parameters W and J upon V_1, V_2, and E_R (see Appendix A and Ref. [18]). Note also that the maximal experimental width observed after expansion of the order of 40 μm corresponds to ~ 80 main lattice sites, much smaller than the phase-space cell, which covers 431 main lattice sites.

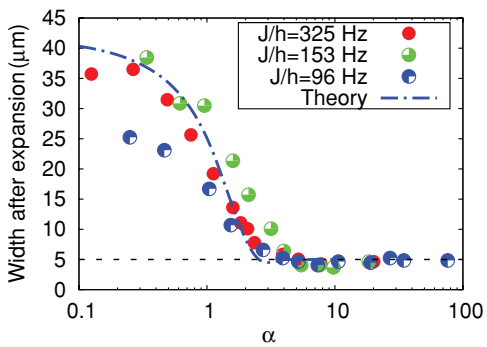

FIG. 3. (Color online) RMS width of a cloud of ^{39}K atoms after $t = 750$ ms of expansion in a (quasi)periodic potential characterized by $\beta = 85/431 = 0.1972, \ldots$ as a function of α. The initial width of the cloud is 5 μm, indicated by a horizontal dashed line. Dots represent the experimental results for different values of J/h (taken from Ref. [3]) and dashed-dots the theory (see text).

IV. COMPARISON WITH THE ANDERSON MODEL

In the previous sections we stress the classical origin of the localization transition and the localized phase in bichromatic potentials. Let us be more explicit, in particular in the comparison with respect to the Anderson model of localization by emphasizing their differences and similarities (comparisons between the quantum motion in disordered and quasiperiodic potentials may also be found in Refs. [17,19,20]).

The original Anderson model of localization [21] with diagonal disorder is described, in 1D, by a Hamitonian similar to Eq. (1). The difference is that the energy of site n, instead of being $\cos(2\pi\beta n)$, is now given by a random variable V_n having, for instance, a uniform distribution between -1 and 1. Then W simply controls the amplitude of the random potential and WV_n has a uniform distribution between $-W$ and W.

If one wishes to follow a semiclassical analysis similar to the previous one but for the Anderson model, the first difficulty is to define appropriately the classical limit. The potential, as defined earlier, is not continuous and has no direct classical limit. One way to get around this difficulty is to smooth the previous random potential, for instance, by convoluting V_n with a Gaussian of width σ

$$V(q) = W \sum_n V_n \frac{e^{-(q-q_n)/2\sigma^2}}{\sqrt{2\pi\sigma^2}}, \qquad (12)$$

where q_n denotes, as in the previous sections, the position of the sites of the discrete lattice separated by a distance λ_1. Then, the classical limit of the Anderson model is described by the Hamiltonian

$$\mathcal{H}(q, p) = 2J\cos(2\pi p/P) + WV(q), \qquad (13)$$

where $P = h/\lambda_1$. The classical phase-space trajectories of such a Hamiltonian are, qualitatively, not very different from those of the quasiperiodic potential in Eq. (3), in particular in the two extreme limits $\alpha \to 0$ and $\alpha \to \infty$ (see Fig. 4): They are given, again, by delocalized constant-p trajectories in the former limit where the kinetic part of the energy dominates over the potential and localized constant-q trajectories in the latter one, where the potential traps the orbits (we are using, as before, the parameter $\alpha = W/J$). The main difference is in the intermediate regime where, for the Anderson model, the classical trajectories are more irregularly shaped and a larger number of separatrices is observed. Thus, as in the quasiperiodic Hamiltonian, in the Anderson model a delocalized to localized crossover is observed classically as α increases.

As we saw in the previous sections, the quasiperiodic case qualitatively follows the classical behavior. For $\alpha < 2$ the kinetic part dominates, the classical trajectories lie above the potential barriers and are delocalized in space. In contrast, at $\alpha = 2$ the last delocalized classical trajectory disappears and all orbits are, for $\alpha > 2$, trapped by the potential barriers and thus are localized in space. Quantum mechanically, a crossover that simply follows this classical behavior is observed from delocalized states that dominate at $\alpha < 2$ to localized ones at

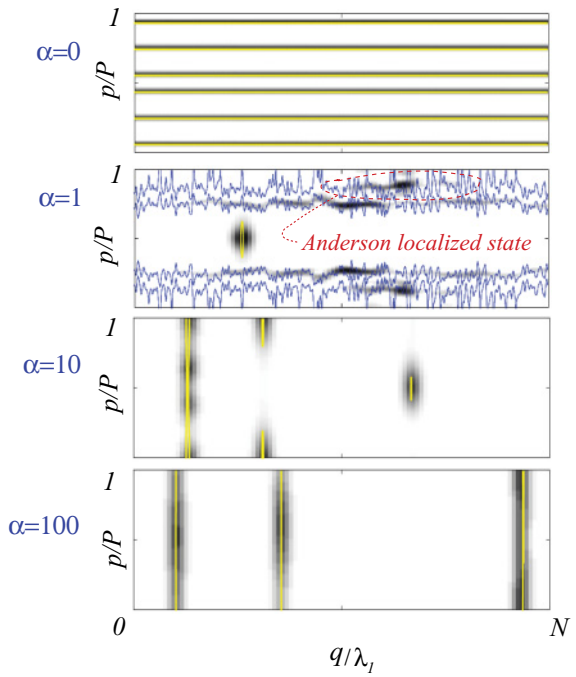

FIG. 4. (Color online) Husimi distributions (gray code) of several eigenstates and their corresponding classical orbits (solid lines) in phase space for the Anderson model with $N = 401$ and $\sigma = \lambda_1$. As α increases the classical model also exhibits a delocalized-localized crossover. Localized quantum eigenstates already exist for $\alpha < 2$ even if the corresponding classical orbits are delocalized in space as shown for $\alpha = 1$.

$\alpha > 2$ (cf. Fig. 3). This behavior contrasts with the Anderson model, where quantum states are localized for arbitrary values of $\alpha > 0$, in spite of having a qualitatively similar classical behavior. Figure 4 illustrates this point by showing several quantum states for different values of α. We numerically diagonalized the Anderson model on a finite chain of $N = 401$ sites with $\vec{\theta} = (0, 0)$ and obtained the classical phase-space orbits from Eq. (13) with $\sigma = \lambda_1$. For the sake of clarity, Fig. 4 does not show all the classical orbits at a given energy but only the ones directly associated to a quantum state. In the two limiting cases, namely $\alpha = 0$ and $\alpha \gg 1$ (here 100), the quantum states are associated to very simple classical orbits (i.e., fully delocalized and fully localized trajectories, respectively). However, at finite α the eigenstates are localized, even those where the energy corresponds to classical orbits above the potential barriers, as shown in Fig. 4 for $\alpha = 1$ (of course the length of the system should be longer than the corresponding localization length). This latter behavior is not observed in the quasiparticle case.

Thus, the main difference between the quantum behavior of the two models is in the range $\alpha < 2$, where the Anderson model, in contrast to the classical behavior (orbits above the barriers), has localized states while the quasiperiodic model follows the behavior of the classical trajectories. For large values of α, the localization in the Anderson model has, as the quasiperiodic potential, a classical interpretation because the classical orbits are themselves localized (e.g., trapped by the potential barriers). In this respect, the nontrivial regime in the Anderson model is the nonclassical localization observed for small values of α, an effect that is absent in the bichromatic potential. A particularly interesting way to stress this difference is to look at the effects of decoherence. It is well known that decoherence drives the system dynamics toward the classical motion by suppressing the interference effects [22]. In the regime $\alpha < 2$, decoherence will therefore destroy localization in the Anderson case leading to a classical diffusion, whereas it will fundamentally not affect the dynamics, aside from quantum corrections, in the quasiperiodic potential. This stresses the differences and similarities between the two models in their quantum and classical behavior.

V. CONCLUSION

In the present article we analyze, using semiclassical methods, the localization transition observed in quasiperiodic potentials. A general analysis of the corresponding Aubry-André Hamiltonian in terms of the commensurability properties of the parameter β is given. Particular attention is devoted to the interpretation of recent cold-atom experiments as well as to a comparison with the 1D Anderson model of localization.

Several extensions and generalizations of the dynamics considered here are of interest, with possible experimental realizations. They are motivated by the possibility of exploring more complex transport effects. Among them, we can mention the possibility of pulsating in time one of the two superimposed potentials, thus introducing chaotic motion in the dynamics described by the kicked Harper Hamiltonian [23]. Along similar lines of research concerning kicked systems, it is worthwhile to mention recent cold-atom experiments that explore the three-dimensional Anderson metal-insulator transition [24]. Another important issue is related to the effects of interactions on the localization properties of quasiperiodic as well as random potentials [20,25].

ACKNOWLEDGMENTS

This work was supported by Grant Nos. ANR-05-Nano-008-02 and ANR-NT05-2-42103 and by the IFRAF Institute.

APPENDIX A: CORRECTION TO THE HAMILTONIAN PARAMETERS

In Ref. [3] they use the following notations. The original Hamiltonian describing the motion of cold atoms in a bichromatic potential is written

$$\hat{H}_B = -\frac{\hbar^2}{2m}\frac{\partial^2}{\partial x^2} + s_1 E_{R_1}\cos^2(k_1 x) + s_2 E_{R_2}\cos^2(k_2 x), \tag{A1}$$

where $k_i = 2\pi/\lambda_i$ and $E_{R_i} = \hbar^2 k_i^2/2m$, $i = 1, 2$, denote the wave numbers and the two recoil energies, respectively. Its reduction to a tight-binding form is expressed as

$$\hat{H} = J\sum_m |w_{m+1}\rangle\langle w_m| + |w_m\rangle\langle w_{m+1}| + W\sum_m \cos(2\pi\beta m)|w_m\rangle\langle w_m|, \tag{A2}$$

where $\beta = \lambda_1/\lambda_2$ (not restricted to [0, [1]). The parameters in (A2), namely J and W, were calculated as follows

$$J = 1.43 s_1^{0.98} \exp(-2.07\sqrt{s_1}), \qquad W = \frac{s_2 E_{R_2}}{2E_{R_1}}, \tag{A3}$$

and thus

$$\alpha = \frac{W}{J} = \frac{\beta^2}{2.86}\frac{s_2}{s_1^{0.98}}\exp(2.07\sqrt{s_1}). \tag{A4}$$

On the other hand, in Ref. [26] the mapping between the two Hamiltonians (A1) and (A2) was studied very carefully to analyze the presence of possible mobility edges due to deviations from the tight-binding approximation. Writing their formulas with the same set of notations as in Ref. [3] yields

$$\alpha = \frac{W}{J} = \frac{\sqrt{\pi}\beta^2}{8}\frac{s_2}{s_1^{3/4}}\exp(2\sqrt{s_1} - \beta^2/\sqrt{s_1}), \tag{A5}$$

which turns out to present significant deviations with respect to Eq. (A4). Indeed, if one takes, for instance, $s_1 = 10$ and $\beta = 1.2$, which are of the order of magnitude of the experimental parameters in Ref. [3], there is about a factor 2 between the two expressions.

APPENDIX B: BARGMAN REPRESENTATION ON THE TORUS

Following Ref. [9], we present here the Bargman's representation on the extended torus. Classically, the two-dimensional toroidal phase space is a periodically repeated cell having sides (Q, P) in suitable coordinates (q, p). The classical dynamics is invariant under translations by the elementary cell. Quantum mechanically, the states of the Hilbert space are required to be periodic functions (up to a phase) under translations defined on an extended torus of size (MQ, P) (M is an arbitrary, strictly positive integer)

$$T_{MQ}|\psi\rangle = e^{i\theta_1}|\psi\rangle, \qquad T_P|\psi\rangle = e^{i\theta_2}|\psi\rangle, \tag{B1}$$

where $\vec{\theta} = (\theta_1, \theta_2)$ are two Bloch phases ranging from 0 to 2π and

$$\hat{T}_Q = \exp(-iQ\hat{p}/\hbar), \qquad \hat{T}_P = \exp(iP\hat{q}/\hbar). \tag{B2}$$

To simultaneously satisfy Eq. (B1) T_Q and T_P must commute. This imposes that the area of the extended phase space, measured in units of Planck's constant h, must be an integer

$$\frac{MQP}{2\pi\hbar} = N. \tag{B3}$$

Thus, the Hilbert space is an N-dimensional space parametrized by $\vec{\theta}$ and denoted $\mathcal{H}_N(\vec{\theta})$. For a fixed area MQP the semiclassical limit $\hbar \to 0$ is equivalent to $N \to \infty$.

For each $\mathcal{H}_N(\vec{\theta})$ one can define normalizable basis states $|q_n, \vec{\theta}\rangle$ and $|p_m, \vec{\theta}\rangle$ in the q and p representations, respectively,

$$|q_n, \vec{\theta}\rangle = \sum_{\nu=-\infty}^{\infty} e^{-i\nu\theta_1}|q_n + \nu MQ\rangle, \quad n = 0, \ldots, N-1,$$
$$|p_m, \vec{\theta}\rangle = \sum_{\nu=-\infty}^{\infty} e^{-i\nu\theta_2}|p_m + \nu P\rangle, \quad m = 0, \ldots, N-1, \tag{B4}$$

where

$$q_n = \frac{MQ}{N}\left(n + \frac{\theta_2}{2\pi}\right), \qquad p_m = \frac{P}{N}\left(m - \frac{\theta_1}{2\pi}\right). \tag{B5}$$

In Eq. (B4), $|q_n + \nu MQ\rangle$ and $|p_m + \nu P\rangle$ are the usual position and momentum eigenstates, respectively, that have to be distinguished with respect to their periodized counterpart, $|q_n, \vec{\theta}\rangle$ and $|p_m, \vec{\theta}\rangle$. The latter states satisfy the boundary conditions in Eq. (B1) and $\langle n, \vec{\theta}|m, \vec{\theta}\rangle = \exp(iq_n p_m/\hbar)/\sqrt{N}$. As Eq. (B5) shows, the arbitrariness in the boundary conditions may be viewed as an arbitrariness under shifts of order $1/N$ in the position of the discrete basis states $|n, \vec{\theta}\rangle$ and $|m, \vec{\theta}\rangle$ with respect to the intervals $q : [0, MQ[$ and $p : [0, P[$, respectively.

Diagonalization of the Harper Hamiltonian in, for instance, the $|q_n, \vec{\theta}\rangle$ basis gives the eigenstates $|\psi_i(\vec{\theta})\rangle = \sum_{n=0}^{N-1}\psi_{i,n}(\vec{\theta})|q_n, \vec{\theta}\rangle$ and $i = 0, \ldots, N-1$, characterized by N complex numbers that satisfy $\sum_{n=0}^{N-1}|\psi_{i,n}(\vec{\theta})|^2 = 1$. An alternative representation is in terms of coherent states [9], or Bargman representation, defined as

$$\psi_i(z, \vec{\theta}) = \sum_{n=0}^{N-1}\psi_{i,n}(\vec{\theta})\langle z|q_n, \vec{\theta}\rangle, \tag{B6}$$

where

$$\langle z|q_n, \vec{\theta}\rangle = (\pi\hbar)^{-1/4}\exp\left\{-\frac{1}{\hbar}\left[\frac{1}{2}(z^2 + q_n^2) - \sqrt{2}zq_n\right]\right\} \times \theta_3\left[-\frac{\theta_1}{2} - i\frac{\pi N}{P}(\sqrt{2}z - q_n)\middle|\frac{iMNQ}{P}\right]. \tag{B7}$$

The complex variable $z = (q - ip)/\sqrt{2}$ denotes the central position of the coherent state and

$$\theta_3(v|\tau) = \sum_{\nu=-\infty}^{+\infty}\exp(i\pi\tau\nu^2 + 2iv\nu), \tag{B8}$$

is the Jacobi θ function [27].

Finally the Husimi representation $W_\psi(z)$ of an eigenstate corresponds to the normalized squared modulus of the coherent state representation

$$W_i(q, p) = \frac{|\psi_i(z, \vec{\theta})|^2}{\langle z|z\rangle} = e^{-|z|^2/\hbar}|\psi_i(z, \vec{\theta})|^2. \tag{B9}$$

[1] S. Aubry and G. André, Ann. Isr. Phys. Soc. **3**, 133 (1980).
[2] J. Billy *et al.*, Nature (London) **453**, 891 (2008).
[3] G. Roati *et al.*, Nature **453**, 895 (2008).
[4] Y. Lahini *et al.*, e-print arXiv:0807.2845 (2008).
[5] M. Ya. Azbel, Phys. Rev. Lett. **43**, 1954 (1979).
[6] I. M. Suslov, Sov. Phys. JETP **56**, 612 (1982).
[7] D. J. Thouless, M. Kohmoto, M. P. Nightingale, and M. den Nijs, Phys. Rev. Lett. **49**, 405 (1982).
[8] M. Wilkinson, Proc. R. Soc. London Ser. A **391**, 305 (1984).
[9] P. Leboeuf and A. Voros, J. Phys. A **23**, 1765 (1990).
[10] J. Kurchan, P. Leboeuf, and M. Saraceno, Phys. Rev. A **40**, 6800 (1989).
[11] P. G. Harper, Proc. Phys. Soc. A **68**, 874 (1955).
[12] N. W. Ashcroft and N. D. Mermin, *Solid State Physics* (Harcourt, Orlando, 1976).
[13] L. G. Yaffe, Rev. Mod. Phys. **54**, 407 (1982).
[14] A. Avila and S. Jitomirskaya, Lecture Notes in Phys. **690**, 5 (2006).
[15] S. Jitomirskaya, Ann. Math. **150**, 1159 (1999).
[16] F. Faure, J. Phys. A **33**, 531 (2000).
[17] C. Aulbach *et al.*, New. J. Phys. **6**, 70 (2004).
[18] M. Modugno, New J. Phys. **11**, 033023 (2009).
[19] S. Aubry and P. Quemerais, in *Low-dimensional Electronic Properties of Molybdenum Bronzes and Oxides* (Kluwer Academic, Dordrecht/Boston/London, 1989) pp. 295–405.
[20] G. Roux, T. Barthel, I. P. McCulloch, C. Kollath, U. Schöllwock, and T. Giamarchi, Phys. Rev. A **78**, 023628 (2008).
[21] P. W. Anderson, Phys. Rev. **109**, 1492 (1958).
[22] In the context of localization, this effect has been experimentally observed for ultracold atoms in a kicked potential in H. Ammann, R. Gray, I. Shvarchuck, and N. Christensen, Phys. Rev. Lett. **80**, 4111 (1998).
[23] P. Leboeuf, J. Kurchan, M. Feingold, and D. P. Arovas, Phys. Rev. Lett. **65**, 3076 (1990).
[24] J. Chabé, G. Lemarié, B. Grémaud, D. Delande, P. Szriftgiser, and J. C. Garreau, Phys. Rev. Lett. **101**, 255702 (2008).
[25] T. Paul, P. Schlagheck, P. Leboeuf, and N. Pavloff, Phys. Rev. Lett. **98**, 210602 (2007); M. Albert, T. Paul, N. Pavloff, and P. Leboeuf, *ibid.* **100**, 250405 (2008); X. Deng, R. Citro, E. Orignac, and A. Minguzzi, Eur. Phys. J. B **68**, 435 (2008).
[26] D. J. Boers, B. Goedeke, D. Hinrichs, and M. Holthaus, Phys. Rev. A **75**, 063404 (2007).
[27] E. T. Whittaker and G. N. Watson, *A Course of Modern Analysis* (Cambridge University Press, Cambridge, England 1965), Chap 21.